Aquaculture 595 (2025) 741491

Contents lists available at ScienceDirect

Aquaculture

journal homepage: www.elsevier.com/locate/aquaculture

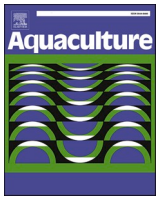

Automated phenotyping empowered by deep learning for genomic prediction of body size in the tiger pufferfish, *Takifugu rubripes*

Zijie Lin [a], Sota Yoshikawa [b], Masaomi Hamasaki [b], Kiyoshi Kikuchi [a], Sho Hosoya [a,*]

[a] *Fisheries Laboratory, University of Tokyo, Hamamatsu, Shizuoka 431-0214, Japan*
[b] *Nagasaki Prefectural Institute of Fisheries, 1551-4, Taira, Nagasaki 851-2213, Japan*

ARTICLE INFO

Keywords:
Computer vision
Low fishmeal diet
Genomic selection
Mask-RCNN

ABSTRACT

Although genomic selection (GS) is accelerating the genetic improvement of economically important traits in aquaculture species, the accurate phenotyping of thousands of individuals remains a bottleneck in GS programs. Computer vision (CV) technologies with the assistance of deep learning may provide a cost-efficient solution for automated phenotyping of fish body size. In this study, we designed a CV-based automated phenotyping system based on the deep learning model Mask R-CNN (region-based convolutional neural networks) and tested its ability to predict standard length (SL) of tiger pufferfish (*Takifugu rubripes*) fed low fishmeal (LFM) diet. Simultaneously, we investigated the impact of the automated phenotyping on genetic parameter estimation and genomic prediction for growth-related traits. We raised a test population ($n = 1001$) that was fed the LFM diet from three months old until harvest at 22 months. Manual phenotyping of the fish was performed at 10-, 14-, 17-, and 22-months-old. At the last two measurement times, images of each fish were collected to train Mask R-CNN for fish detection and pixel-level segmentation of the fish body excluding the tail fin. An automated phenotyping pipeline combining the trained Mask R-CNN and standard CV algorithms were designed to estimate SL. We found a high correlation (0.965–0.971) and low relative difference (0.015–0.027) between the CV-derived and manually measured SL, indicating high precision of our CV system. A high correlation (0.912–0.956) was also observed between CV-derived body area and manual body weight. The heritability estimations and genomic predictions on manual SLs were conducted using a Genomic Best Linear Unbiased Prediction (GBLUP) model using a total of 16,471 single nucleotide polymorphism (SNP). Estimated heritability at the four sampling points ranged from 0.573 to 0.622, and the predictive ability of genomic prediction for harvest size was 0.627. These values are comparable to those reported in previous studies collected from the population fed a normal fishmeal diet. Our heritability estimation and genomic prediction derived from automated SL measurements differed negligibly to those based on manual measurements. This finding indicates the utility of our CV-based automated phenotyping system for GS breeding programs.

1. Introduction

Genomic selection (GS) is a state-of-the-art selective breeding technology that makes use of phenotypes and high-density genome-wide DNA markers to select broodstock with high genetic potential (Meuwissen et al., 2001). This technology is now playing a central role in selective breeding and the genetic improvement of farmed fish, improving the productivity and sustainability of aquaculture industries. (Houston et al., 2020; Costello et al., 2020; Gephart et al., 2020; Naylor et al., 2021). In aquaculture, GS has been applied to economically important species such as salmonids (Odegård et al., 2014; Yáñez et al., 2014), shrimp (*Litopenaeus vannamei*) (Wang et al., 2019), large yellow croaker (*Larimichthys crocea*) (Bai et al., 2022; Dong et al., 2016), European seabass (*Dicentrarchus labrax*) (Besson et al., 2022), gilthead sea bream (*Sparus aurata*) (Palaiokostas et al., 2016), and the tiger pufferfish (*Takifugu rubripes*) (Hosoya et al., 2021; Lin et al., 2020; Yoshikawa et al., 2021). However, the substantial costs associated with genotyping and phenotyping of hundreds or thousands of individuals impose a significant bottleneck in the GS process (Houston et al., 2020). Improvements in next-generation sequencing technologies, coupled with the advantage of aquaculture species in which low density SNPs (2–5 K SNPs) can capture substantial linkage disequilibrium within

* Corresponding author.
E-mail address: ahosoya@mail.ecc.u-tokyo.ac.jp (S. Hosoya).

https://doi.org/10.1016/j.aquaculture.2024.741491
Received 15 April 2024; Received in revised form 23 July 2024; Accepted 14 August 2024
Available online 15 August 2024
0044-8486/© 2024 The Authors. Published by Elsevier B.V. This is an open access article under the CC BY license (http://creativecommons.org/licenses/by/4.0/).

populations, have reduced this problem by markedly reducing genotyping expenses (Kriaridou et al., 2020). On the other hand, it is expected that use of automated phenotyping systems based on computer vision (CV) offers a cost-efficient solution to high-throughput phenotyping (Houston et al., 2020). The increasing affordability of electro-optical sensors and computing resources has further bolstered the potential for CV-based automated phenotyping in aquaculture (Saberioon et al., 2017).

To date, CV-based automated phenotyping technologies have predominantly been used in plants and livestock (Awada et al., 2018; Bhat et al., 2020; Koltes et al., 2019; Pérez-Enciso and Steibel, 2021); however, there is increasing use of these technologies in aquaculture. For example, shrimps (*Litopenaeus vannamei* and *Penaeus monodon*), pearl oysters (*Pinctada maxima*) (Zenger et al., 2019), Jade perch (*Scortum barcoo*) (Viazzi et al., 2015), rainbow trout (*Oncorhynchus mykiss*) (Miranda and Romero, 2017), and Bluefin Tuna (*Thunnus Thynnus*) (Muñoz-Benavent et al., 2018), have been analyzed by CV-based automated phenotyping and the results have indicated its high accuracy. CV-based technologies and machine learning algorithms require a comprehensive understanding of the underlying principles that govern image patterns, and also require a step-by-step simplification of images into the desired features through appropriate mathematical algorithms. However, it is not a simple matter to translate complex patterns from fish images into simple mathematics, and this has limited the wider adoption of CV technologies. In contrast, CV in combination with deep learning may circumvent such limitations and enable the direct mapping of input images to desired outputs using extensive image data without the need for detailed prior knowledge (O' Mahony et al., 2019). Deep learning, a rapidly evolving branch of artificial intelligence (AI), seeks to emulate the ability of the human brain to extract features from visual information, and can result in superior performance across a range of intricate CV tasks. Thus, deep learning-based CV has the potential to outperform other techniques in terms of accuracy for high-throughput phenotyping (Kamilaris and Prenafeta-Boldú, 2018; Liakos et al., 2018). Mask R-CNN is an algorithm of R-CNN (region-based convolutional neural networks) that enables detection, classification, and precise segmentation (He et al., 2017). It has been demonstrated to have practical applications in fisheries such as reducing catches of undersized fish (Garcia et al., 2020), evaluating fillet freshness (Prasetyo et al., 2020), monitoring fish behavior (Chang et al., 2021), and body size measurements (Yu et al., 2020). A combination of Mask R-CNN inference and standard CV algorithms has recently been employed for automated phenotyping in a pedigree-based selective breeding program for pacu (*Piaractus mesopotamicus*) (Freitas et al., 2023). The results of these various studies in important aquaculture species highlight the potential of image data and deep learning in cost-effective high-throughput phenotyping to enhance genetic gains in aquaculture breeding programs. To confirm this potential, it will be essential to demonstrate that the estimated phenotypes have sufficient accuracy for genomic predictions for aquaculture species; to date such confirmation has rarely been performed.

In this study, we examined the feasibility of high-throughput phenotyping using a customized CV system employing a trained Mask R-CNN model for measuring standard length (SL) of the tiger pufferfish and explored the utility of CV-derived SL data in genomic prediction. The tiger pufferfish is a major aquaculture species in East Asian countries including Japan, and total production of species is high among mariculture species and is rapidly increasing (Wang et al., 2022; Hamasaki et al., 2017; Ministry of Agriculture, Forestry and Fisheries (MAFF), Japan, 2023). In addition, this species is also known as fugu, a model fish for genetic and genomic research in vertebrates (Aparicio et al., 2002; Hamasaki et al., 2017; Kabir et al., 2022; Kai et al., 2011; Zhao et al., 2024). Several GS breeding programs have been undertaken to improve growth-related traits (i.e., SL and body weight), testes weights, and resistance to the gill parasite *Heterobothrium okamotoi* (Hosoya et al., 2021; Lin et al., 2020). Application of CV-based automated phenotyping should increase the efficiency of such breeding programs. One difficulty with regard to farmed tiger pufferfish is that they exhibit complex artificial morphological variations in the mouth area due to the trimming or extraction of their teeth to prevent damage from cannibalistic behavior (Hosoya et al., 2017); for deep learning to be of value, it must overcome these challenges.

Here, we raised a test population of the tiger pufferfish fed a low fishmeal (LFM) diet for 19 months from three months of age until harvest (i.e., 22 months old). Standard length was manually measured at four time points; image data were collected at the third and fourth sampling time and used to train a Mask R-CNN model for fish body detection. A customized image processing pipeline combining Mask R-CNN inference with traditional CV algorithms was developed to assess the accuracy of SL estimation. We then investigated the impact of automated measurements on genetic parameters (i.e., heritability and prediction accuracy of genomic selection for standard length) by comparing the results obtained from manual measurements with those derived from automated measurements. We also discussed the impact of long-term use of the LFM diet on the growth performance and the genetic parameters, a critical issue for the sustainable growth of the aquaculture industry.

2. Material and methods

2.1. Production of test fish

The test fish for this study were produced at the Nagasaki Prefectural Institute of Fisheries (NPIF, Nagasaki, Japan). These fish were part of a population used in our previous study (Lin et al., 2024): this F_1 population (PopLFM1) was generated through artificial mating involving 35 males and 29 females with a total of 807 crosses. These fish were produced following Chuda et al. (1998), Miyaki et al. (1998) and Yoshikawa et al. (2020) with modification. Broodfish, with an average body weight of 2.88 ± 0.52 kg, were induced ovarian maturation and ovulation by implanting cholesterol pellets containing LHRHa (des-Gly^{10}[D-Ala^6]--luteinizing hormone-releasing hormone ethylamide, Sigma-Aldrich, St. Louis, MO, USA) into their back muscle at a dose of 400 μg LHRHa per 1 kg body weight. Gametes were stripped from the broodfish following anesthetization using 200 mg/L of 2-phenoxyethanol and used for artificial fertilization following a nearly full-factorial mating design, as detailed in Supplementary File S1 of Lin et al., 2024. Fertilized eggs from the same dam (maternal half-sib group) were pooled and incubated in one-ton tanks per half-sib group with flow-through seawater and aeration. After hatching, larvae from all half-sib groups were mixed and reared in a 15-ton tank until three months of age. The capacity of the tank was increased to 30-ton at 6 months-of-old, 50-ton at 9-months-old, and 100-ton at 12-months-old, and maintained at 100-ton until the final sampling. The rearing conditions and management procedures for these fish were the same as in the previous study (Lin et al., 2024). In brief, experimental tanks were provided with ultraviolet-sterilized seawater and were aerated. After hatching, the fish were nourished with nutrient-enriched live L-type rotifers, *Artemia* nauplii, and standard extruded pellets diet, characterized by a high fishmeal content (77%) (Lavelarva and Junior, Hayashikane Sangyo Co., Ltd., Yamaguchi, Japan), depending on their developmental stage. At three-months-old, 1001 fish were randomly collected from the holding tank. Each fish was uniquely identified using a passive integrated transponder (PIT) tag that was embedded in the left side of the body trunk; fin samples were obtained from each fish for DNA extraction. The fish were then fed the low fishmeal (LFM) diet described by Lin et al. (2022) at 1.5% of fish weight 3–5 times a week. Fin samples were also collected from the broodfish ($n = 64$) and their siblings ($n = 20$) for genotyping.

2.2. Manual phenotyping and image data collection

Manual phenotyping was performed at four intervals: at 7 months

(on the 198th day), 11 months (on the 319th day), 14 months (on the 422nd day), and 19 months (on the 569th day) from the initiation of the LFM dietary treatment. At each assessment except the final sampling, SLs (SL_1, SL_2, SL_3) and body weights (BW_1, BW_2, BW_3) were manually measured for each test fish using a measuring tape and an electric scale, respectively, following anesthesia with 200 mg/L of 2-phenoxyethanol. At the final sampling, each test fish was euthanized with 600 mg/L of 2-phenoxyethanol. At this point, measurements including SL_4, BW_4, and gonad weight (male, $GW_{♂}$; female, $GW_{♀}$) were made, and phenotypic sex was determined. Note that testis weight is an important economic trait for this species as the testis is a favored delicacy in Japan (Yoshikawa et al., 2020). Corrected body weight was calculated by subtracting gonad weight (male, $BW_{♂4} = BW_4 - GW_{♂}$; female, $BW_{♀4} = BW_4 - GW_{♀}$).

At the third and fourth sampling, digital images of each fish (along with a scale ruler) were captured using a fixed photography setup (see Fig. 1). In brief, the camera was mounted on a photographic tripod to ensure the camera lens remained parallel with the table. On the table, a waterproof blue sheet served as the background for the fish image. The distance between the camera lens and the table was maintained at 127 cm so that the camera's field of view covered the blue sheet. Lighting was adjusted using two floodlights [Iwasaki Electric, PRF350WD100V (FLOOD)]. A 30 cm metric ruler was used as a scale reference to convert pixel length in the images of the fish to actual lengths. The left side of each fish was photographed in the center of the image background, with a number card placed on the upper-left side.

Two digital cameras were employed: a DSLR-A550 (Sony, Tokyo, Japan) with a wide-angle prime lens [Minolta, AF 50 Macro 1:3.5(32)]; and a customized Pi-camera. The latter is an assembly of a high-quality camera with a 16 mm C-mount lens and a single-board computer (Raspberry Pi 3 Model B+, Raspberry Pi Foundation, Cambridge, UK) running on the Raspberry Pi operating system. Custom GUI software was developed for photography and image calibration based on the Python/OpenCV-3.4.1 camera calibration procedure (GitHub repository: https://github.com/gglinzijie/Automatic_phenotyping_fugu/blob/main/gui_test.py). Data collection was primarily carried out using the Sony camera at the third (14th month; dataset name Sony3rd, $n = 954$) and fourth sampling points (19th month; dataset name Sony4th, $n = 937$). A subset of the samples was used for photograph data collection with the Pi-camera during the third sampling point (dataset name Pi3rd, $n = 105$). The images from the Sony3rd and Sony4th datasets were resized from 2288 × 1580 pixels to 572 × 380 pixels using the cv2.resize function in Python (v3.4.1) and saved in JPG format (sRGB, 350 dpi). The images from Pi3rd were stored in JPG format (1872 × 964 pixels, sRGB, and 96 dpi). Figure sizes were further adjusted during the pre-processing stage, ensuring that no bias resulted from differences in the saved image sizes between the two cameras in subsequent analyses.

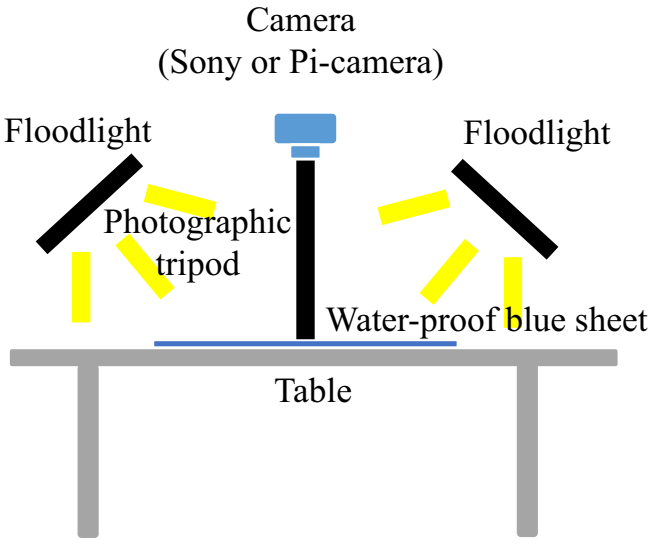

Fig. 1. Illustration of the customized photography system.
A digital camera (Sony, DSLR-A550) or the customized Pi-camera was mounted on a photographic tripod at a fixed distance of 127 cm above the table. Two floodlights (PRF350WD100V, Iwasaki Electric, Japan) were positioned beside the camera. A waterproof blue sheet was placed on the table as the background for the fish image. (For interpretation of the references to colour in this figure legend, the reader is referred to the web version of this article.)

2.3. Image annotation

Image annotation is a critical step in this study, serving a dual role in mapping pixel coordinates of images to centimeters and in training the deep learning model. Point annotation of ruler images and contour annotation of fish images were carried out using "*point*" and "*polygon region shape*" functions implemented in the VGG image annotator (v2.0.9) (Dutta and Zisserman, 2019). A demonstration of the annotation process can be found in Fig. 2.

In the case of images containing the metric ruler, we annotated zero mark (x_1, y_1) and 30 cm mark (x_2, y_2), and calculated pixel distance as

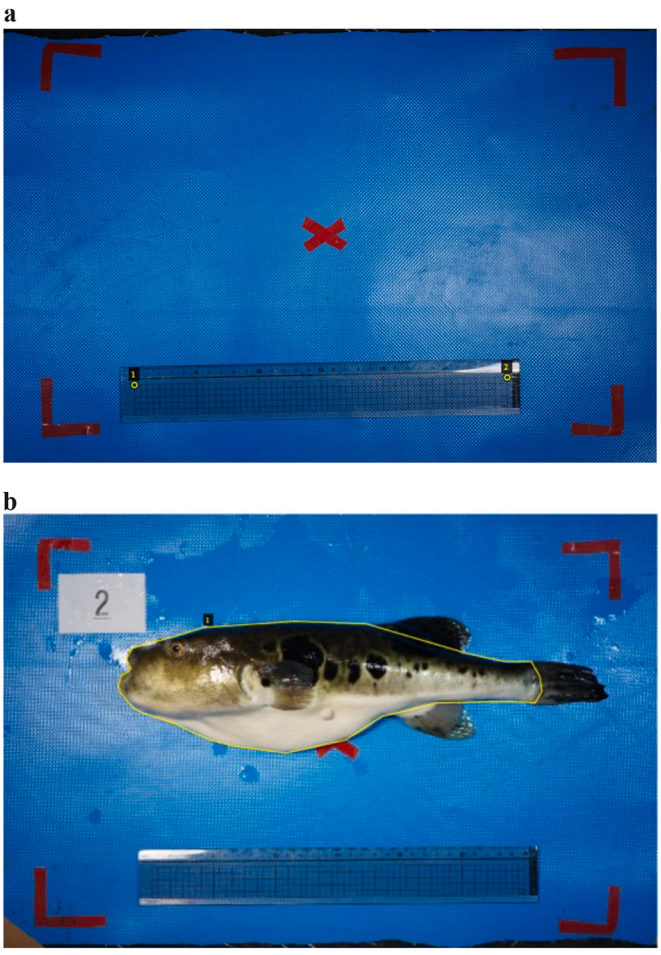

Fig. 2. An example image of image annotation with VGG image annotator (v2.0.9).
(**a**) Point annotation of ruler images: two points (yellow circles) were marked on the metric ruler in the image using the "*point*" option; the pixel coordinates of these points were used for converter estimation. (**b**) Contour annotation of fish images: vertices of the polygonal contour of the fish body, excluding fins (yellow polygon) were annotated using the "*polygon region shape*" option and the polygonal contour was labeled as "*fish_body*". The pixel coordinates of the annotated vertices and the labels were used for training the deep learning model. (For interpretation of the references to colour in this figure legend, the reader is referred to the web version of this article.)

follows:

$$d_{pixel\_30cm} = \sqrt{(x_1 - x_2)^2 + (y_1 - y_2)^2}$$

Given that the digital camera, lens, and table remained fixed during photography, the conversion factor for mapping pixel coordinates in ruler images to actual fish images remains consistent. Therefore, the pixel distance of each fish image (d_{pixel}) can be converted to real-world metric (d_{cm}) as follows:

$$d_{cm} = d_{pixel} \times 30 / d_{pixel\_30cm}$$

For each fish image, the vertices of the polygonal contour (representing the fish body excluding fins) were annotated, and this polygonal contour was labeled as "*fish_body*" for training the Mask R-CNN. All annotation information was saved as JavaScript Object Notation (JSON) format.

2.4. Mask R-CNN training and automated phenotyping

The trained Mask R-CNN model serves as a foundational element within the automated phenotyping pipeline, with the expectation of conducting inferences on unlabeled fish images. This includes the detection of the tiger pufferfish, precise localization of the fish via bounding boxes, and the generation of per-pixel segmentation masks for the fish body (excluding fins) (Fig. 3a). In summary, the Mask R-CNN model operates in two stages; it initially extracts features and proposes candidate objects (region proposals), and subsequently, it conducts bounding box regression, object classification, and region mask estimation on the candidate objects. The Mask R-CNN model was trained using open-source Python scripts (*model.py*, *config.py*, *utils.py*, and *visualize.py*; https://github.com/matterport/Mask_RCNN, accessed on April 1, 2019) based on TensorFlow (v1.6.0) and Keras (v2.1.5), with some minor modifications. A Docker environment was employed for training

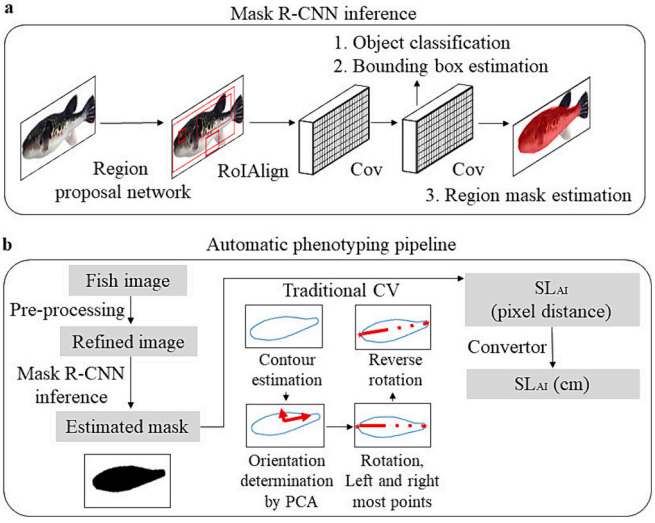

Fig. 3. Demonstration of (**a**) Mask R-CNN inference and (**b**) a customized image processing pipeline.
(**a**) The Mask R-CNN model extracts features using a region proposal network and proposes the candidate objects. RoIAlign and convolutional layers (Cov) were used to further extract features from these candidate objects. Finally, object classification, bounding box regression, and region mask estimation were performed on each candidate object. (**b**) The fish image was pre-processed to refine the image, and subsequently used to estimate the mask of the fish body, excluding fins, by the trained Mask R-CNN model. Standard length (SL_{AI}) was obtained from the mask image using traditional computer vision (CV) algorithms, including contour estimation, orientation determination by principal component analysis (PCA), and estimation of SL_{AI} in pixel distance. Finally, the pixel distance of SL_{AI} was converted to cm.

(https://hub.docker.com/r/waleedka/modern-deep-learning), inference, and the automated phenotyping pipeline, all on the Ubuntu 16.04 LTS operating system.

To estimate the SL and body area measurements from the collected fish images (SL_{AI} and BA_{AI}), we designed a customized image processing pipeline that combined Mask R-CNN inference with traditional CV algorithms, primarily implemented using Python/cv2 (v3.4.1) (Fig. 3b). In brief, the input image underwent pre-processing, yielding a refined image that was subsequently used to detect the tiger pufferfish and estimate the mask of the fish body (excluding fins) through the trained Mask R-CNN model. The estimated mask was further processed by traditional CV algorithms to derive the pixel distance for SL_{AI}. Finally, the pixel distance and area were converted to real-world units (cm and cm^2). Detailed coding information can be found in Supplementary File S1. All customized Python scripts, docker file, and the trained model (mask_rcnn_shapes_0030.h5) are available in our GitHub repository (see https://github.com/gglinzijie/Automatic_phenotyping_fugu).

2.5. Genotyping for genetic analysis

Genomic DNAs were extracted from caudal fin clips of the 64 parent individuals, 20 of their siblings, and 1000 progeny using the Gentra Puregene Tissue Kit (QIAGEN, Hilden, Germany) following the manufacturer's instructions. Although 1001 fish were initially included in the progeny sample, one died before the first sampling point. The DNA samples were used for genotyping by the GRAS-Di (Genotyping by Random Amplicon Sequencing, Direct) method (Hosoya et al., 2019; Yoshikawa et al., 2021). GRAS-Di is a random PCR-based genotyping by sequencing technology, and characterized by its simplicity in library construction; sequencing library are constructed by sequential two PCR step. In brief, the DNA template was initially amplified by a first PCR using Illumina Nextera adaptor sequences and 3-base random oligomers. Subsequently, the diluted PCR products were barcoded through a second PCR using Illumina multiplexing 8-base dual indices and P7/P5 adapter sequences. Three libraries were prepared and sequenced on the Illumina Novaseq 6000 sequencer, employing the NovaSeq 6000 S4 reagent kit (Illumina, San Diego, USA). Library preparation and sequencing procedures were performed by Eurofins Genomics, Inc. (Tokyo, Japan).

Raw sequencing reads were trimmed using Trim Galore-0.6.6 (Krueger) with the following parameters: -length 100 -stringency 10 -paired. With this step, low-quality bases (Q score below 20), adapter sequences, and sequences overlapping the adapter sequences (10 base pairs) were trimmed; both reads in pair should be longer than 100 bps after trimming, otherwise discarded. Validation of reads pair was also performed. Trimmed reads were then mapped to a reference fugu genome (FUGU5/fr3) using BWA-MEM (v0.7.17-r1188) (Li, 2013). Reads with mapping quality values (MAPQ) below 10 and those with any bits set in "2308" in the FLAG field were removed using samtools (v1.9) (Li et al., 2009). Genotype calling for each sample was carried out using GATK (v4.1.6.0) (Poplin et al., 2017). The *HaplotypeCaller* tool was used with the following options: *–output-mode EMIT_ALL_CONFIDENT_SITES -ERC GVCF –stand-call-conf 30*. The obtained gVCF files were combined via GATK *GenomicsDBImport*, and joint genotyping was carried out using GATK *GenotypeGVCFs*. Variant filtering was performed using vcftools (v0.1.5) with the parameters: *–remove-indels, –-min-alleles 2, –-*max-*alleles 2, –-minQ 20, –-min-meanDP 20, –-minDP 10, –-max-meanDP 300, –-maf 0.01, –-hwe 0.05, and –max-missing 0.7*. Missing genotypes were subsequently imputed using LinkImpute (Money et al., 2015).

2.6. Genetic analysis

As population structure can bias the results, we inferred population sub-structures using a principal component analysis (PCA) within the progeny samples with complete phenotype and genotype records (n = 936) prior to the genetic analysis. The PCA was performed using the

decomposition.PCA function implemented in the Python/scikit-learn-0.23.2 package with default settings. Scatter plots were generated using a customized Python script based on the matplotlib-3.3.1 package.

We then estimated narrow-sense heritability under a Genomic Best Linear Unbiased Prediction (GBLUP) model: $\mathbf{y} = \mathbf{u} + \mathbf{Za} + \mathbf{e}$, where y is the vector of phenotypic values; **u** is the vector of population mean (the fixed effect); **Z** is a design matrix connecting individual record and additive genetic effects (**a**) for each individual, **a** follows the normal distribution $\sim N(0, \mathbf{G}\sigma_a^2)$ where **G** is the realized genomic relationship matrix; **e** is a vector of residuals follows normal distribution $\sim N(0, \sigma_e^2)$. The **G** matrix was built from 16,471 SNPs using *A.mat* function and the model was solved using the restricted maximum likelihood (REML) algorithm with the *kin.blup* function both implemented in R/rrBLUP-4.6 (Endelman, 2011). Concurrently, a genomic estimated breeding value (GEBV) for each individual was obtained from the results provided by the same function. Changes in GEBVs of each individual over the experimental period was assessed using Pearson's correlation (*r*) between GEBVs for SL_i. Predictive ability and prediction accuracy was evaluated based on a five-fold cross-validation scheme (Hosoya et al., 2018). The samples were randomly and equally divided into five subsets, one for testing and the remaining four for training. The phenotypic values for both traits in the test set were masked, and the regression model was trained using the training set. For each trait, GEBVs of the test set were predicted, and predictive ability was calculated as the Pearson's correlation (*r*) between GEBVs and observed values in the test set. Prediction accuracy, determined as predictive ability divided by square root of estimated heritability, was also calculated. This process was repeated by rotating the test sets among the five subsets, and the average of predictive abilities and prediction accuracies was obtained. This cross-validation procedure was repeated five times to yield the mean and standard error of the mean (S.E.) for both metrics.

Genetic correlation between SL at the four sampling points (SLi) was calculated by a multivariate linear mixed model: $\mathbf{y}_i = \mathbf{u}_i + \mathbf{Z}_i\mathbf{a}_i + \mathbf{e}_i$, where $\mathbf{y}_i$ is a vector of phenotypes for trait SL_i; $\mathbf{u}_i$ represents fixed effects of population mean. $\mathbf{Z}_i$ is an incidence matrix for random effects $\mathbf{a}_i$, which follow a multivariate normal distribution as $MVN(0, \mathbf{K} \otimes \mathbf{G})$; The residuals (**e**) follow $MVN(0, \mathbf{R} \otimes \mathbf{I})$, where **K** and **R** are the variance-covariance matrices of random effects and residuals for the two traits, respectively; **G** is the additive genetic relationship matrix constructed as previously described; **I** is the identity matrix; $\otimes$ means the operation of Kronecker product. The model was solved using the *mmer* function in R/sommer-4.0.1 (Covarrubias-Pazaran, 2018) to solve the equations. The genetic correlation (r_g) was computed as: $r_g = \sigma_{g_i g_j} / \sqrt{\sigma_{g_i}^2 \sigma_{g_j}^2}$, where $\sigma_{g_i}^2$ and $\sigma_{g_j}^2$ is the genetic variance for trait SL_i; $\sigma_{g_i g_j}$ is the genetic covariance between two traits.

3. Results

3.1. Summary statistics of manually collected phenotypes

An initial population of 1001 fish were fed the LFM diet for the 19 months duration of the experiment; 936 fish survived to the final sampling interval. The phenotypes of these fish are summarized in Table 1 and their SLs are shown in Fig. 4 (the full records for each fish are available in Supplementary Table S1). High Pearson's correlation coefficients ($r = 0.849$–0.947) were found between SLs at the different sampling points. The 936 fish alive at the end of the experiment included 459 females, 466 males, 10 hermaphrodites, and one individual whose gender and GW were not recorded. The mean GW of males ($GW_♂$) was in the normal range (Table 1), suggesting that long-term feeding with the LFM diet did not have an adverse effect on the gonadal development of male tiger pufferfish as well. We observed sex differences in GWs and corrected body weights due to differences in sex-related maturation ages; however, there were no significant differences between the average BW_4 of males and that of females (ANOVA test, $p = 0.154$).

Table 1
Summary statistics for manually collected phenotypes ($n = 936$).

Trait	Mean ± S.D.	Range	Coefficient of variation (%)
SL_1 (cm)	24.18 ± 1.70	18.5–28.6	7.03
SL_2 (cm)	26.29 ± 1.84	19.50–31.4	7.00
SL_3 (cm)	30.69 ± 2.13	22.1–36.0	6.94
SL_4 (cm)	35.56 ± 2.55	25.1–41.6	7.17
BW_1 (g)	452.2 ± 96.5	195–780	21.35
BW_2 (g)	579.3 ± 127.0	230–1048	21.93
BW_3 (g)	821.8 ± 170.1	285–1345	20.70
BW_4 (g)	1524.3 ± 360.3	450–2920	23.64
$GW_♂$ (g)	231.6 ± 103.9	1–602	44.85
$BW_{♂4}$ (g)	1308.5 ± 282.5	513–2371	21.59
$GW_♀$ (g)	31.9 ± 26.2	0.4–186	82.23
$BW_{♀4}$ (g)	1474,3 ± 338.2	449–2404	22.94

SL_1, SL_2, SL_3 and SL_4 (BW_1, BW_2, BW_3 and BW_4) are standard length (body weight) at 7 months (198 days), 11 months (319 days), 14 months (422 days), and 19 months (569 days) from the start of the long-term feeding treatment, respectively.
S.D.: standard deviation.
Coefficient of variation (%): S.D. divided by mean.
$GW_♂$: gonad weight for male.
$GW_♀$: gonad weight for female.
$BW_{♂4} = BW_4 - GW_♂$.
$BW_{♀4} = BW_4 - GW_♀$.

3.2. Performance evaluation of the trained mask R-CNN model and automated phenotyping

The trained Mask R-CNN model successfully detected fish bodies and provided precise segmentation masks for the body of each fish image with high average Intersection over Union (IoU) values ranging from 0.947 to 0.953 (Table 2). To automatically estimate SL_{AI} and BA_{AI}, the customized pipeline was applied to all fish images from Sony3rd, Sony4th, and Pi3rd (Table 2 and Supplementary Table S1). The Sony3rd/Pi3rd and Sony4th that were used for SL_{AI} estimation were collected at the same sampling points as SL_3 and SL_4, respectively. We found high correlations between SL_{AI} and the corresponding SL_i (all images, 0.965–0.971; test set, 0.967–0.989). Additionally, average absolute differences between SL_{AI} and SL_i were very low (all images, 0.513–0.819 cm; test set, 0.561–0.916 cm) as were relative differences (all images, 0.015–0.027; test set, 0.016–0.032; Tables 2 and 3). A high correlation was found between SL_{AI} estimated from Sony3rd and Pi3rd for the same individuals ($n = 105$, $r = 0.969$). Strong linear relationship was also confirmed between SL_{AI} and SL_i from regression coefficients (SL_3, $\beta = 0.986$, $p < 0.001$; SL_4, $\beta = 0.979$, $p < 0.001$). These findings indicate that automated phenotyping provides measurements that closely and accurately approximate manual measurements. A high correlation was also observed between BA_{AI} and BW_i (Sony3rd, $r = 0.956$; Sony4th, $r = 0.916$); this correlation was higher than that between SL_{AI} and BW_i (Sony3rd, $r = 0.912$; Sony4th, $r = 0.892$) suggesting that BA_{AI} is more effective in predicting BW than SL_{AI}.

3.3. Genotyping

Genomic DNAs were extracted from 1084 samples from the 64 broodfish, 20 of their siblings, and 1000 test fish; these DNAs were subjected to GRAS-Di sequencing (Supplementary Table S2). On average, approximately 4,529,807 ± 494,169 (S.D.) raw reads were obtained per individual. After quality-trimming, the mean number of reads per individual was 3,557,154 ± 344,917. The retained reads were then mapped to a reference fugu genome (FUGU5/fr3) for SNP calling. Following SNP calling, filtration, and imputation, a dataset of 16,471 SNPs was obtained for each fish.

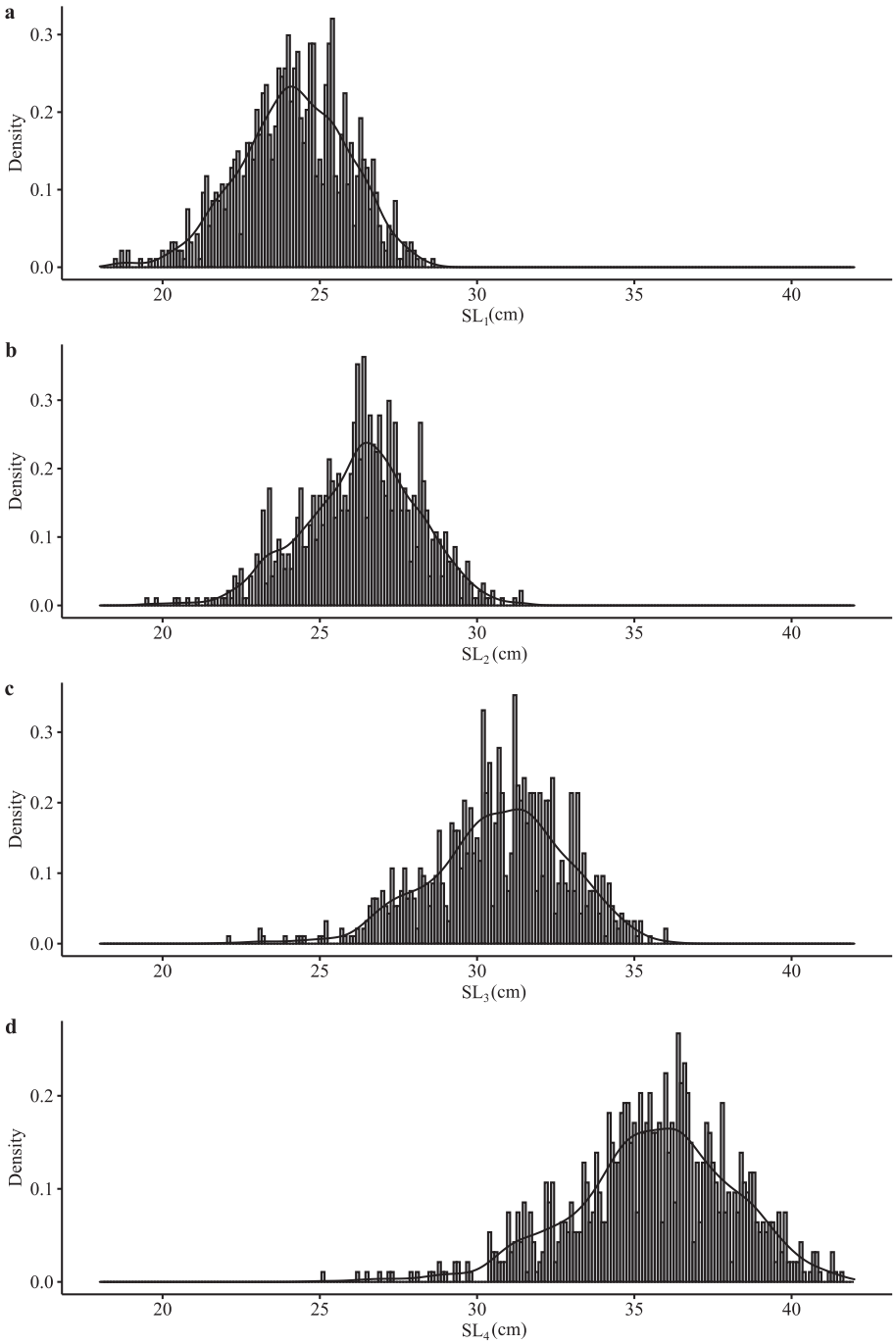

Fig. 4. Histograms of standard lengths.
Histograms with the kernel density of the standard length (cm) of tiger pufferfish at four different time points: a) SL_1 (7 months), b) SL_2 (11 months), c) SL_3 (14 months), and d) SL_4 (19 months).

3.4. Assessment of population structure

The population structure was analyzed using the dataset from the 936 progenies for which phenotype (SL and BW) and genotype records were complete. This analysis was carried out using a PCA based on the 16,471 genome-wide SNPs (Fig. 5). Consistent with the crossing scheme, we did not find distinct clusters or substantial stratification in this population. This finding indicates that potential biases stemming from population structure were minimal in the subsequent genetic analysis.

3.5. Genetic analysis on the manual phenotyping data

Heritability estimates for SL manually collected at the four sampling points were obtained using the GBLUP model. Moderate heritability was observed at each time point: SL_1, 0.573; SL_2, 0.621; SL_3, 0.622; and SL_4, 0.617 (estimated variance components were detailed in Supplementary Table S3). Additionally, high genetic correlations (r_g = 0.917–0.974) were observed between each manual measurement of SL_i (Supplementary Table 4). The heritability estimate for testis weight is lower (h^2 = 0.499) compared to that of the previous study (h^2 = 0.686) (Hosoya et al., 2021).

Predictive abilities for SL at harvest size (SL_4, 22-months-old) were

Table 2
Evaluation metrics of Mask R-CNN inference and image-based phenotyping pipeline for standard length (average ± S.D.)

Dataset	Group	IoU	Absolute difference (cm)	Relative difference	*r*
Sony3rd	All images	0.949 ± 0.008	0.513 ± 0.348	0.017 ± 0.011	0.971
(*n* = 954)	Training set	0.949 ± 0.008	0.502 ± 0.342	0.016 ± 0.011	0.970
	Validation set	0.950 ± 0.008	0.552 ± 0.347	0.018 ± 0.011	0.977
	Test set	0.947 ± 0.009	0.561 ± 0.389	0.019 ± 0.013	0.974
Sony4th	All images	0.949 ± 0.009	0.541 ± 0.401	0.015 ± 0.011	0.968
(*n* = 937)	Training set	0.949 ± 0.009	0.541 ± 0.402	0.015 ± 0.012	0.967
	Validation set	0.951 ± 0.008	0.520 ± 0.349	0.015 ± 0.010	0.976
	Test set	0.951 ± 0.008	0.557 ± 0.438	0.016 ± 0.012	0.967
Pi3rd	All images	0.949 ± 0.008	0.819 ± 0.497	0.027 ± 0.016	0.965
(*n* = 105)	Training set	0.949 ± 0.009	0.764 ± 0.504	0.025 ± 0.016	0.958
	Validation set	0.953 ± 0.008	1.179 ± 0.385	0.039 ± 0.012	0.983
	Test set	0.948 ± 0.013	0.916 ± 0.401	0.032 ± 0.014	0.989

IoU: average intersection over union of Mask R-CNN inference on fish body
r: Pearson's correlation coefficient between manually collected SL and CV-derived SL
Absolute difference: absolute difference between manual and automated measurements
Relative difference: absolute difference divided by manual measurements.

Table 3
Summary statistics for manual measurements of standard length (SL_i) and automated measurements of standard length (SL_{AI}), and body area (BA_{AI}) (average ± S.D.)

Dataset	Group	SL_i (cm)	SL_{AI} (cm)	BA_{AI} (cm^2)
Sony3rd	All images	30.65 ± 2.15	30.99 ± 2.19	182.82 ± 27.64
(*n* = 954)	Training set	30.74 ± 2.09	31.07 ± 2.11	183.56 ± 27.14
	Validation set	30.60 ± 2.42	30.45 ± 2.43	176.39 ± 27.64
	Test set	30.54 ± 2.31	30.93 ± 2.45	183.27 ± 28.93
Sony4th	All images	35.57 ± 2.56	35.73 ± 2.58	271.95 ± 43.81
(*n* = 937)	Training set	35.54 ± 2.54	35.70 ± 2.56	271.46 ± 43.36
	Validation set	35.43 ± 2.57	35.70 ± 2.64	270.15 ± 45.03
	Test set	35.89 ± 2.69	36.04 ± 2.71	277.77 ± 46.20
Pi3rd	All images	30.50 ± 2.13	31.27 ± 2.21	187.27 ± 27.91
(*n* = 105)	Training set	30.75 ± 1.98	31.45 ± 2.09	190.08 ± 26.73
	Validation set	30.45 ± 1.87	31.63 ± 2.01	188.06 ± 26.38
	Test set	28.67 ± 2.66	29.59 ± 2.73	165.03 ± 30.19

moderate (0.627 ± 0.006) (Supplementary Table 3). The predictive abilities at other sampling points were similar to that of SL_4: SL_1, 0.587 ± 0.006; SL_2, 0.643 ± 0.005; and SL_3, 0.625 ± 0.006. The predictive ability and prediction accuracy for testis weight at harvest were 0.537 ± 0.010 and 0.801 ± 0.015, respectively.

3.6. Impact of automated phenotyping on genetic analysis

To assess the impact of automated high-throughput phenotyping on genetic analysis, SL_{AI} (Sony3rd and Sony4th) was used for heritability estimation and genomic prediction; the results were compared with values obtained from SL_i at the same sampling point (Table 4).

Variance components (see Supplementary Table S3) and heritability estimates for SL_{AI} (Sony3rd, 0.620; Sony4th, 0.626) were similar to those from manual measurements. The differences in predictive abilities were marginal between SL_{AI} (Sony3rd, 0.627 ± 0.006; Sony4th, 0.629 ± 0.006) and manual measurements. Most importantly, correlation between GEBVs for SL_3 and Sony3rd and between SL_4 and Sony4th were strong ($r = 0.982$ and 0.982, respectively; Fig. 6). All these comparisons consistently supported the interpretation that automated phenotyping had a minimal impact on the estimation of genetic parameters and was of practical use for genomic prediction for SL in tiger pufferfish.

4. Discussion

In this study, we investigated the applicability of CV-based automated phenotyping using Mask R-CNN for estimating body size in tiger pufferfish. The high correlation in IoU values and the small relative differences between manual measurements confirmed the accuracy of our pipeline, suggesting its suitability for automated, high-throughput measurement of SL in this species. We further assessed use of our automated phenotyping pipeline on heritability estimation and genomic prediction, and found that the automated phenotyping approach gave comparable results to manual phenotyping. This finding highlights the effectiveness of the image-based phenotyping pipeline for GS breeding programs.

We trained the Mask R-CNN model to act as the basis of our automated phenotyping pipeline. The trained Mask R-CNN was successful in estimating the pixel-level segmentation mask of the fish body, excluding the tail fin, with a high average IoU value (0.947–0.953). We also attempted to improve the accuracy of mask segmentation. For example, we found it difficult to accurately determine the contour of the mouth, the start point for SL measurements. Cultured tiger pufferfish often have irregularities in the shape of their mouth, due to tooth trimming or extraction to reduce physical damage from cannibalism. These changes make it difficult to accurately determine the contour of the tip of the fish mouth. To improve accuracy, we added more annotation points to define the mouth, thereby providing additional guidance to the model during training. We also increased the resolution of contour prediction from 28 × 28 pixels to 56 × 56 pixels by modifying the architecture of the Mask R-CNN (Supplementary File S1), i.e., by adding a transposed convolution layer at the end of the mask segmentation branch. These adjustments improved the accuracy of the model in detecting and segmenting the difficult areas. Our findings indicate that the model training strategy, i.e., the annotation process, model structure, and training procedure, will need to be refined several times according to the morphological characteristics of the test species to meet the high accuracy requirements of GS breeding programs.

One limitation of the trained deep learning model was that it was less robust when extrapolating from one dataset to another. When we trained the model using only the Sony3rd dataset, consisting of 17-month-old fish, and predicted fish body segmentation in the Sony4th dataset (22-months-old fish), an IoU value of 0.873 was obtained compared to the values obtained for its own dataset (0.947–0.953). This limitation is particularly important for breeding programs that involve genetic improvements in body size over multiple generations. In addition, domestication and breeding programs may inadvertently alter fish morphology (Luo et al., 2021; Pulcini et al., 2013), and therefore could affect the accuracy of a trained Mask R-CNN model over time. To address these problems, training data will need to be collected from fish of a wide range of sizes, including those larger than regular harvest size. Continuous updating of the training dataset and evaluation of accuracy is recommended.

In this study, we used cultured tiger pufferfish reared on LFM diet for 19 months until harvest (3 to 22-months-old). The availability of LFM diets and their impact on selective breeding are critically important for the sustainable growth of aquaculture, given the shortage and rising prices of fishmeal. This is particularly important for carnivorous fish such as the tiger pufferfish which requires a high proportion of fishmeal (70–80%) in their feed (Cottrell et al., 2020; Lin et al., 2022). Previously, we found that an LFM diet, in which a large amount of fishmeal (> 50%)

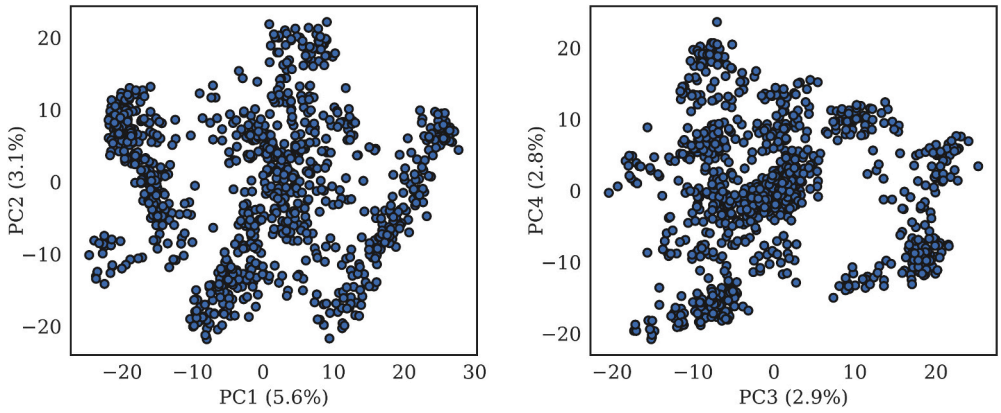

Fig. 5. Principal component analysis of population structure.
Principal component analysis of population structure based on genomic information (n = 936); the left panel shows the first two principal components (PCs), and right panel shows the third and the fourth PCs.

Table 4
Comparison of the results from genetic analysis based on manual and automated measurements.

Trait	h^2	Predictive ability	Prediction accuracy	r_{GEBVs}
SL_3	0.622	0.620 (± 0.006)	0.786 (± 0.008)	0.982
SL_{AI} (Sony3rd)	0.620	0.627 (± 0.006)	0.796 (± 0.008)	
SL_4	0.627	0.625 (± 0.006)	0.789 (± 0.008)	0.982
SL_{AI} (Sony4th)	0.626	0.629 (± 0.006)	0.795 (± 0.008)	

Predictive ability and prediction accuracy were determined by five-fold cross validation with GBLUP model.
r_{GEBVs}: Pearson's r between GEBVs estimated by GBLUP.

was replaced by yeast-based protein, was compatible with growth improvement (Lin et al., 2022). We also confirmed the feasibility of using GS to increase body size and heterobothriosis resistance in juvenile tiger pufferfish fed this diet for a short period (three to four months) (Lin et al., 2024). In this study, we revealed that long-term use of the LFM diet was not detrimental on the growth of the pufferfish as their body size and testes weights were similar or even superior to the results obtained previously (mean SL: 33.99 ± 2.38 cm, mean BW: 1156.6 ± 271.2 g, and testes weight: 94.2 ± 66.6 g) (Hosoya et al., 2021). In addition, the heritability, predictive ability, and prediction accuracy for SL_4 (h^2 = 0.627, ability = 0.625, and accuracy = 0.789) was comparable or higher than that reported for the population fed standard diets at harvest (h^2 = 0.538, ability = 0.551, and accuracy = 0.751) (Hosoya et al., 2021). These results indicate that the LFM diet did not have any adverse effects on heritability or GEBV estimation and supports the possibility of genomic selection for SL of the tiger pufferfish fed the LFM diet. On the other hand, under low fishmeal feeding conditions, the heritability of testis weight (h^2 = 0.499) was lower compared to that obtained under normal conditions (0.686) (Hosoya et al., 2021). This may be due to the differences in the genetic structure of the test populations, but it also suggests the potential impact of gene-diet interaction as suggested previously (Lin et al., 2024). The existence of gene-diet interaction has also been suggested in other farmed fish, including amago salmon (*Oncorhynchus masou ishikawae*) (Yamamoto et al., 2016), rainbow trout (*Oncorhynchus mykiss*) (Le Boucher et al., 2011) and European sea bass (*Dicentrarchus labrax*) (Le Boucher et al., 2013). Given the importance, further investigation of gene-diet interactions on economic traits is needed.

While automated phenotyping has advanced rapidly in plant breeding (Bhat et al., 2020; Moreira et al., 2020), particularly in the context of GS breeding programs for wheat (Crain et al., 2018; Shabannejad et al., 2020), evaluation of automated phenotyping in GS breeding programs is still in its infancy in aquaculture. Automated

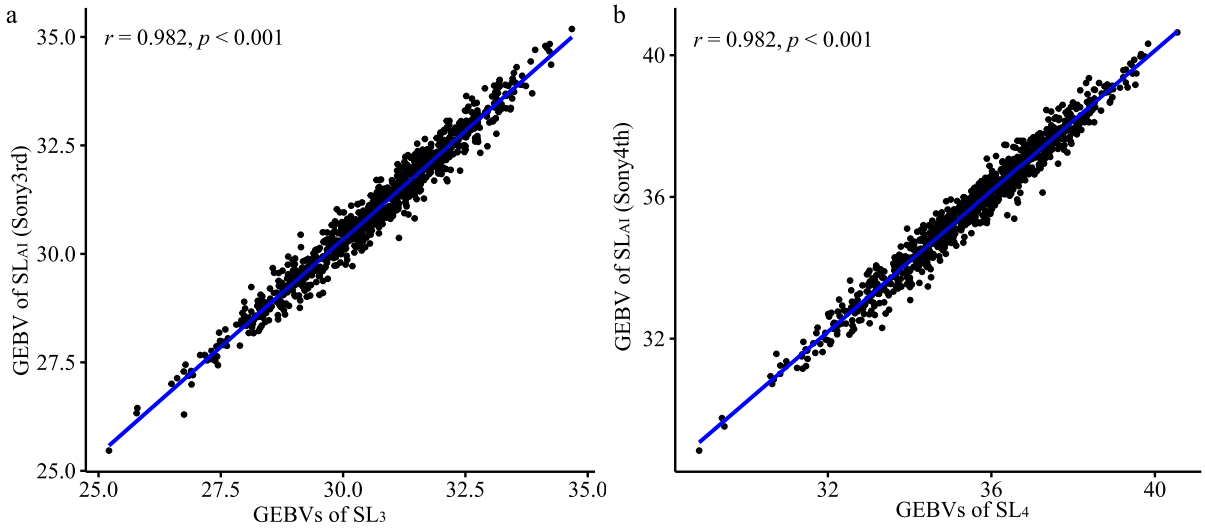

Fig. 6. Scatter diagrams of GEBVs for manually and automated measurements.
Scatter diagrams of GEBVs for manually and automated measurements of standard length at (**a**) the third (SL_3 and Sony3rd) and (**b**) the fourth (SL_4 and Sony4th) sampling points. Pearson's correlation coefficients (r) and the p-value for the correlation between them are included in each panel.

phenotyping can help reduce labor costs and also subjectivity and/or recording errors associated with manual measurements, especially in a large-scale breeding program that requires phenotyping of thousands of individuals from multiple families (Pérez-Enciso and Steibel, 2021; Toda et al., 2021). Our study highlights the feasibility of automated phenotyping for GS in aquaculture breeding programs, and the system developed in this study (the combination of Mask R-CNN inference with the traditional CV algorithm) provided an accurate and cost-effective approach for measuring fish body size. The programming difficulty of implementing deep learning inference on a single-board computer has been greatly reduced; this will accelerate the development of automated measurement technologies and significantly improve aquaculture production when combined with other technologies, including selective breeding.

5. Conclusions

Our results confirmed the reliability and practicality of the automated phenotyping system with CV technologies employing a Mask R-CNN model for genetic analyses within the framework of GS for the tiger pufferfish. Our results also underscore the importance of continuous model evaluation and data collection for the application of the CV-based automated phenotyping in aquaculture breeding programs. Additionally, the feasibility of GS for harvest body size in fish fed an LFM diet was demonstrated. This research provides valuable insights into improving automated phenotyping systems and understanding the influence of LFM diets on heritability and genomic prediction in the tiger pufferfish.

Ethics approval

All experiments performed in this study were approved by the local Fish Care Committee of NPIF (#NPIF-0001) and carried out in accordance with the Guidelines and Regulations for Fish Experimentation at NPIF

Funding

This work was supported by Japan Society for the Promotion of Science (JSPS) Grant-in-Aid for Scientific Research (B) (21H02279) granted to S.H., JST (JST-Mirai Program, JPMJMI18CH and JPMJMI21C1), Japan, granted to K.K.

CRediT authorship contribution statement

Zijie Lin: Writing – original draft, Visualization, Software, Investigation, Data curation. **Sota Yoshikawa:** Validation, Resources, Investigation. **Masaomi Hamasaki:** Resources. **Kiyoshi Kikuchi:** Writing – review & editing, Supervision, Funding acquisition, Conceptualization. **Sho Hosoya:** Writing – review & editing, Validation, Project administration, Methodology, Investigation, Conceptualization.

Declaration of competing interest

The authors declare the following financial interests/personal relationships which may be considered as potential competing interests.

Sho HOSOYA reports financial support was provided by Japan Society for the Promotion of Science. Kiyoshi KIKUCHI reports financial support was provided by JST-Mirai Program. If there are other authors, they declare that they have no known competing financial interests or personal relationships that could have appeared to influence the work reported in this paper.

Data availability

The image data and annotations will be made available upon request. The Python scripts and the trained Mask R-CNN model are available at GitHub repository (https://github.com/gglinzijie/Automatic_phenotyping_fugu). The genotyping sequence reads have been deposited in the DDBJ Sequence Read Archive (DRA Accession: DRA016345).

Acknowledgements

We would like to thank Dr. Toshiyuki Yamada and Mr. Kanta Mori from NIPF, and Dr. Goro Yoshizaki and Dr. Ryosuke Yazawa from Tokyo University of Marine Science and Technology for their valuable comments.

Appendix A. Supplementary data

Supplementary data to this article can be found online at https://doi.org/10.1016/j.aquaculture.2024.741491.

References

Aparicio, S., Chapman, J., Stupka, E., Putnam, N., Chia, J., Dehal, P., Christoffels, A., Rash, S., Hoon, S., Smit, A., Gelpke, M.D.S., Roach, J., Oh, T., Ho, I.Y., Wong, M., Detter, C., Verhoef, F., Predki, P., Tay, A., Lucas, S., Richardson, P., Smith, S.F., Clark, M.S., Edwards, Y.J.K., Doggett, N., Zharkikh, A., Tavtigian, S.V., Pruss, D., Barnstead, M., Evans, C., Baden, H., Powell, J., Glusman, G., Rowen, L., Hood, L., Tan, Y.H., Elgar, G., Hawkins, T., Venkatesh, B., Rokhsar, D., Brenner, S., 2002. Whole-genome shotgun assembly and analysis of the genome of Fugu rubripes. Science 297 (5585), 1301–1310. https://doi.org/10.1126/science.1072104.

Awada, L., Phillips, P.W.B., Smyth, S.J., 2018. The adoption of automated phenotyping by plant breeders. Euphytica 214, 148. https://doi.org/10.1007/s10681-018-2226-z.

Bai, Y.L., Wang, J.Y., Zhao, J., Ke, Q.Z., Qu, A., Deng, Y.C., Zeng, J.J., Gong, J., Chen, J., Pan, Y., Chi, H.S., Gong, H., Zhou, T., Xu, P., 2022. Genomic selection for visceral white-nodules diseases resistance in large yellow croaker. Aquaculture 559, 738421. https://doi.org/10.1016/j.aquaculture.2022.738421.

Besson, M., Morvezen, R., Bestin, A., François, Y., Bajek, A., Brunier, J., Morin, T., Vandeputte, M., Dupont-Nivet, M., Izquierdo, M., Barkas, D., Haffray, P., 2022. Selective breeding for survival to *Vibrio harveyi* in European seabass (*Dicentrarchus labrax*) is robust to different feeding environments. In: World Congress on Genetics Applied to Livestock Production. Wageningen Academic Publishers, pp. 688–691. https://doi.org/10.3920/978-90-8686-940-4_159.

Bhat, J.A., Deshmukh, R., Zhao, T., Patil, G., Deokar, A., Shinde, S., Chaudhary, J., 2020. Harnessing high-throughput phenotyping and genotyping for enhanced drought tolerance in crop plants. J. Biotechnol. 324, 248–260. https://doi.org/10.1016/j.jbiotec.2020.11.010.

Chang, C.C., Wang, Y.P., Cheng, S.C., 2021. Fish segmentation in sonar images by mask R-CNN on feature maps of conditional random fields. Sensors 21 (22), 7625. https://doi.org/10.3390/s21227625.

Chuda, H., Hara, Y., Miyaki, K., Matsuyama, M., 1998. Development of methods for the induction of gonadal maturation and effective insemination in the cultured tiger puffer *Takifugu rubripes*. Bull. Nagasaki Pref. Inst. Fish. 24, 15–25. In Japanese (English abstract). https://agriknowledge.affrc.go.jp/RN/2010622041.

Costello, C., Cao, L., Gelcich, S., Cisneros-Mata, M., Free, C.M., Froehlich, H.E., Golden, C.D., Ishimura, G., Maier, J., Macadam-Somer, I., Mangin, T., Melnychuk, M.C., Miyahara, M., de Moor, C.L., Naylor, R., Nøstbakken, L., Ojea, E., O'Reilly, E., Parma, A.M., Plantinga, A.J., Thilsted, S.H., Lubchenco, J., 2020. The future of food from the sea. Nature 588, 95–100. https://doi.org/10.1038/s41586-020-2616-y.

Cottrell, R.S., Blanchard, J.L., Halpern, B.S., Metian, M., Froehlich, H.E., 2020. Global adoption of novel aquaculture feeds could substantially reduce forage fish demand by 2030. Nat. Food. 1, 301–308. https://doi.org/10.1038/s43016-020-0078-x.

Covarrubias-Pazaran, G., 2018. Software update: Moving the R package sommer to multivariate mixed models for genome-assisted prediction. bioRxiv 354639. https://doi.org/10.1101/354639.

Crain, J., Mondal, S., Rutkoski, J., Singh, R.P., Poland, J., 2018. Combining high-throughput phenotyping and genomic information to increase prediction and selection accuracy in wheat breeding. Plant Genome 11 (1). https://doi.org/10.3835/plantgenome2017.05.0043.

Dong, L., Xiao, S., Chen, J., Wan, L., Wang, Z., 2016. Genomic selection using extreme phenotypes and pre-selection of SNPs in large yellow croaker (*Larimichthys crocea*). Mar. Biotechnol. 18 (5), 575–583. https://doi.org/10.1007/s10126-016-9718-4.

Dutta, A., Zisserman, A., 2019. The VIA annotation software for images, audio and video. In: Proceedings of the 27th ACM International Conference on Multimedia (MM '19), Nice, France. ACM, New York, NY, USA. https://arxiv.org/pdf/1904.10699v3.pdf.

Endelman, J.B., 2011. Ridge regression and other kernels for genomic selection with R package rrBLUP. Plant Genome 43, 250–255. https://doi.org/10.3835/plantgenome2011.08.0024.

Freitas, M.V., Lemos, C.G., Ariede, R.B., Agudelo, J.F.G., Neto, R.R.O., Borges, C.H.S., Mastrochirico, V.A., Porto-Foresti, F., Iope, R.L., Batista, F.M., Brega, J.R.F., Hashimoto, D.T., 2023. High-throughput phenotyping by deep learning to include body shape in the breeding program of pacu (*Piaractus mesopotamicus*). Aquaculture 562, 738847. https://doi.org/10.1016/j.aquaculture.2022.738847.

Garcia, R., Prados, R., Quintana, J., Tempelaar, A., Gracias, N., Rosen, S., Vågstøl, H., Løvall, K., 2020. Automatic segmentation of fish using deep learning with application to fish size measurement. ICES J. Mar. Sci. 77 (4), 1354–1366. https://doi.org/10.1093/icesjms/fsz186.

Gephart, J.A., Golden, C.D., Asche, F., Belton, B., Brugere, C., Froehlich, H.E., Fry, J.P., Halpern, B.S., Hicks, C.C., Jones, R.C., Klinger, D.H., Little, D.C., McCauley, D.J., Thilsted, S.H., Troell, M., Allison, E.H., 2020. Scenarios for global aquaculture and its role in human nutrition. Rev. Fish. Sci. Aquac. 29, 122–138. https://doi.org/10.1080/23308249.2020.1782342.

Hamasaki, M., Takeuchi, Y., Yazawa, R., Yoshikawa, S., Kadomura, K., Yamada, T., Miyaki, K., Kikuchi, K., Yoshizaki, G., 2017. Production of tiger puffer *Takifugu rubripes* offspring from triploid grass puffer *Takifugu niphobles* parents. Mar. Biotechnol. 19 (6), 579–591. https://doi.org/10.1007/s10126-017-9777-1.

He, K., Gkioxari, G., Dollár, P., Girshick, R., 2017. Mask R-CNN. IEEE Trans. Pattern Anal. Mach. Intell. 42 (2), 386–397. https://doi.org/10.1109/TPAMI.2018.2844175.

Hosoya, S., Hirase, S., Kikuchi, K., Nanjo, K., Nakamura, Y., Kohno, H., Sano, M., 2019. Random PCR-based genotyping by sequencing technology GRAS-Di (genotyping by random amplicon sequencing, direct) reveals genetic structure of mangrove fishes. Mol. Ecol. Res. 19, 1153–1163. https://doi.org/10.1111/1755-0998.13025.

Hosoya, S., Kikuchi, K., Nagashima, H., Onodera, J., Sugimoto, K., Satoh, K., Matsuzaki, K., Yasugi, M., Nagano, A.J., Kumagayi, A., Ueda, K., Kurokawa, T., 2017. Genomic selection in aquaculture breeding programs. Bull. FRA 45, 35–39. https://doi.org/10.1002/9781118782392.ch21.

Hosoya, S., Kikuchi, K., Nagashima, H., Onodera, J., Sugimoto, K., Satoh, K., Matsuzaki, K., Yasugi, M., Nagano, A.J., Kumagayi, A., Ueda, K., Kurokawa, T., 2018. Assessment of genetic diversity in Coho salmon (*Oncorhynchus kisutch*) populations with no family records using ddRAD-seq. BMC Res. Notes 11, 548. https://doi.org/10.1186/s13104-018-3663-4.

Hosoya, S., Yoshikawa, S., Sato, M., Kikuchi, K., 2021. Genomic prediction for testes weight of the tiger pufferfish, *Takifugu rubripes*, using medium to low density SNPs. Sci. Rep. 11 (1), 1–10. https://doi.org/10.1038/s41598-021-99829-1.

Houston, R.D., Bean, T.P., Macqueen, D.J., Gundappa, M.K., Jin, Y.H., Jenkins, T.L., Selly, S.L.C., Martin, S.A.M., Stevens, J.R., Santos, E.M., Davie, A., Robledo, D., 2020. Harnessing genomics to fast-track genetic improvement in aquaculture. Nat. Rev. Genet. 21, 389–409. https://doi.org/10.1038/s41576-020-0227-y.

Kabir, A., Ieda, R., Hosoya, S., Fujikawa, D., Atsumi, K., Tajima, S., Nozawa, A., Koyama, T., Hirase, S., Nakamura, O., Kadota, M., Nishimura, O., Kuraku, S., Nakamura, Y., Kobayashi, H., Toyoda, A., Tasumi, S., Kikuchi, K., 2022. Repeated translocation of a supergene underlying rapid sex chromosome turnover in pufferfish. Proc. Natl. Acad. Sci. USA 119 (23), e2121469119. https://doi.org/10.1073/pnas.2121469119.

Kai, W., Kikuchi, K., Tohari, S., Chew, A.K., Tay, A., Fujiwara, A., Hosoya, S., Suetake, H., Naruse, K., Brenner, S., Suzuki, Y., Venkatesh, B., 2011. Integration of the genetic map and genome assembly of fugu facilitates insights into distinct features of genome evolution in teleosts and mammals. Genome Biol. Evol. 3, 424–442. https://doi.org/10.1093/gbe/evr041.

Kamilaris, A., Prenafeta-Boldú, F.X., 2018. Deep learning in agriculture: a survey. Comput. Electron. Agric. 147, 70–90. https://doi.org/10.1016/j.compag.2018.02.016.

Koltes, J.E., Cole, J.B., Clemmens, R., Dilger, R.N., Kramer, L.M., Lunney, J.K., McCue, M.E., McKay, S.D., Mateescu, R.G., Murdoch, B.M., Reuter, R., Rexroad, C.E., Rosa, G.J.M., Serão, N.V.L., White, S.N., Woodward-Greene, M.J., Worku, M., Zhang, H., Reecy, J.M., 2019. A vision for development and utilization of high-throughput phenotyping and big data analytics in livestock. Front. Genet. 10, 1197. https://doi.org/10.3389/fgene.2019.01197.

Kriaridou, C., Tsairidou, S., Houston, R.D., Robledo, D., 2020. Genomic prediction using low density marker panels in aquaculture: performance across species, traits, and genotyping platforms. Front. Genet. 11, 124. https://doi.org/10.3389/fgene.2020.00124.

Le Boucher, R., Quillet, E., Vandeputte, M., Lecalvez, J.M., Goardon, L., Chatain, B., Médale, F., Dupont-Nivet, M., 2011. Plant-based diet in rainbow trout (*Oncorhynchus mykiss* Walbaum): Are there genotype-diet interactions for main production traits when fish are fed marine vs. plant-based diets from the first meal? Aquaculture 321, 41–48. https://doi.org/10.1016/j.aquaculture.2011.08.010.

Le Boucher, R., Vandeputte, M., Quillet, E., Ruelle, F., Vergnet, A., Kaushik, S., Allamellou, J.M., Médale, F., Chatain, B., 2013. Genotype by diet interactions in European sea bass (*Dicentrarchus labrax* L.): Nutritional challenge with totally plant-based diets. Jour. Anim. Sci. 91, 44–56. https://doi.org/10.2527/jas.2012-5311.

Li, H., 2013. Aligning sequence reads, clone sequences and assembly contigs with BWA-MEM. arXiv 1303.3997v2. doi:10.48550/arXiv.1303.3997.

Li, H., Handsaker, B., Wysoker, A., Fennell, T., Ruan, J., Homer, N., Marth, G., Abecasis, G., Durbin, R., 2009. The sequence alignment/map format and SAMtools. Bioinformatics 25, 2078–2079. https://doi.org/10.1093/bioinformatics/btp352.

Liakos, K.G., Busato, P., Moshou, D., Pearson, S., Bochtis, D., 2018. Machine learning in agriculture: a review. Sensors 18 (8), 2674. https://doi.org/10.3390/s18082674.

Lin, Z., Hosoya, S., Sato, M., Mizuno, N., Kobayashi, Y., Itou, T., Kikuchi, K., 2020. Genomic selection for heterobothriosis resistance concurrent with body size in the tiger pufferfish, *Takifugu rubripes*. Sci. Rep. 10, 19976. https://doi.org/10.1038/s41598-020-77069-z.

Lin, Z., Yoshikawa, S., Hamasaki, M., Koyama, T., Kikuchi, K., Hosoya, S., 2022. Effects of low fishmeal diets on growth performance, blood chemical composition, parasite resistance, and gene expression in the tiger pufferfish, *Takifugu rubripes*. Aquaculture 560, 738484. https://doi.org/10.1016/j.aquaculture.2022.738484.

Lin, Z., Yoshikawa, S., Hamasaki, M., Kikuchi, K., Hosoya, S., 2024. Heritability and predictive ability for the heterobothriosis resistance and growth performance in the tiger pufferfish Takifugu rubripes fed standard or low fishmeal diets. Aquaculture 588, 740909. https://doi.org/10.1016/j.aquaculture.2024.740909.

Luo, M.K., Lu, G.Q., Yin, H.R., Wang, L.M., Atuganile, M., Dong, Z.J., 2021. Fish pigmentation and coloration: molecular mechanisms and aquaculture perspectives. Rev. Aquac. 13 (4), 2395–2412. https://doi.org/10.1111/raq.12583.

Meuwissen, T.H.E., Hayes, B.J., Goddard, M.E., 2001. Prediction of total genetic value using genome-wide dense marker maps. Genet 157 (4), 1819–1829. https://doi.org/10.1093/genetics/157.4.1819.

Ministry of Agriculture, Forestry and Fisheries (MAFF), Japan, 2023. Sea Aquaculture Production by Major Fish Species (accessed 3 January 2024). https://www.e-stat.go.jp/stat-search/file-download?statInfId=000040067404&fileKind=0/.

Miranda, J.M., Romero, M., 2017. A prototype to measure rainbow trout's length using image processing. Aquac. Eng. 76, 41–49. https://doi.org/10.1016/j.aquaeng.2017.01.003.

Miyaki, K., Chuda, H., Watanabe, T., Mizuta, K., Tsukashima, Y., Yoshida, N., Tabeta, O., 1998. Treatment of tiger puffer, *Takifugu rubripes*, eggs with tannic acid to eliminate their adhesiveness for seed propagation. Suisanzoushoku 46, 97–100 in Japanese with English abstract.

Money, D., Gardner, K., Migicovsky, Z., Schwaninger, H., Zhong, Y., Myles, S., 2015. LinkImpute: Fast and accurate genotype imputation for nonmodel organisms. G3-GENES. GENOM. GENET. 5, 2383–2390. https://doi.org/10.1534/g3.115.021667.

Moreira, F.F., Oliveira, H.R., Volenec, J.J., Rainey, K.M., Brito, L.F., 2020. Integrating high-throughput phenotyping and statistical genomic methods to genetically improve longitudinal traits in crops. Front. Plant Sci. 11, 681. https://doi.org/10.3389/fpls.2020.00681.

Muñoz-Benavent, P., Andreu-García, G., Valiente-González, J.M., Atienza-Vanacloig, V., Puig-Pons, V., Espinosa, V., 2018. Enhanced fish bending model for automatic tuna sizing using computer vision. Comput. Electron. Agric. 150, 52–61. https://doi.org/10.1016/j.compag.2018.04.005.

Naylor, R.L., Hardy, R.W., Buschmann, A.H., Bush, S.R., Cao, L., Klinger, D.H., Little, D.C., Lubchenco, J., Shumway, S.E., Troell, M., 2021. A 20-year retrospective review of global aquaculture. Nature 591, 551–563. https://doi.org/10.1038/s41586-021-03308-6.

O' Mahony, N., Campbell, S., Carvalho, A., Harapanahalli, S., Hernandez, G.V., Krpalkova, L., Riordan, D., Walsh, J., 2019. Deep learning vs. traditional computer vision. In: Kacprzyk, J. (Ed.), Advances in Intelligent Systems and Computing. Springer, pp. 128–144.

Odegård, J., Moen, T., Santi, N., Korsvoll, S.A., Kjøglum, S., Meuwissen, T.H.E., 2014. Genomic prediction in an admixed population of Atlantic salmon (*Salmo salar*). Front. Genet. 5, 402. https://doi.org/10.3389/fgene.2014.00402.

Palaiokostas, C., Ferraresso, S., Franch, R., Houston, R.D., Bargelloni, L., 2016. Genetics of resistance to photobacteriosis in gilthead sea bream (*Sparus aurata*) using 2b-RAD sequencing. G3-Genes. Genom. Genet 6 (11), 3693–3700. https://doi.org/10.1534/g3.116.035220.

Pérez-Enciso, M., Steibel, J.P., 2021. Phenomes: the current frontier in animal breeding. Genet. Sel. Evol. 53, 22. https://doi.org/10.1186/s12711-021-00618-1.

Poplin, R., Ruano-Rubio, V., DePristo, M.A., Fennell, T.J., Carneiro, M.O., Auwera, G.A. V.D., Kling, D.E., Gauthier, L.D., Levy-Moonshine, A., Roazen, D., Shakir, K., Thibault, J., Chandran, S., Whelan, C., Lek, M., Gabriel, S., Daly, M.J., Neale, B., MacArthur, D.G., Banks, E., 2017. Scaling accurate genetic variant discovery to tens of thousands of samples. bioRxiv 201178. https://doi.org/10.1101/201178.

Prasetyo, E., Suciati, N., Fatichah, C., 2020. A comparison of YOLO and mask R-CNN for segmenting head and tail of fish, 2020. In: 4th International Conference on Informatics and Computational Sciences (ICICoS), Semarang, Indonesia, pp. 1–6. https://doi.org/10.1109/ICICoS51170.2020.9299024.

Pulcini, D., Wheeler, P.A., Cataudella, S., Russo, T., Thorgaard, G.H., 2013. Domestication shapes morphology in rainbow trout *Oncorhynchus mykiss*. J. Fish Biol. 82 (2), 390–407. https://doi.org/10.1111/jfb.12002.

Saberioon, M., Gholizadeh, A., Cisar, P., Pautsina, A., Urban, J., 2017. Application of machine vision systems in aquaculture with emphasis on fish: state-of-the-art and key issues. Rev. Aquac. 9, 369–387. https://doi.org/10.1111/raq.12143.

Shabannejad, M., Bihamta, M.R., Majidi-Hervan, E., Alipour, H., Ebrahimi, A., 2020. A simple, cost-effective high-throughput image analysis pipeline improves genomic prediction accuracy for days to maturity in wheat. Plant Methods 16, 146. https://doi.org/10.1186/s13007-020-00686-2.

Toda, Y., Kaga, A., Kajiya-Kanegae, H., Hattori, T., Yamaoka, S., Okamoto, M., Tsujimoto, H., Iwata, H., 2021. Genomic prediction modeling of soybean biomass using UAV-based remote sensing and longitudinal model parameters. Plant Genome 14, e20157. https://doi.org/10.1002/tpg2.20157.

Viazzi, S., Van Hoestenberghe, S., Goddeeris, B.M., Berckmans, D., 2015. Automatic mass estimation of jade perch *Scortum barcoo* by computer vision. Aquac. Eng. 64, 42–48. https://doi.org/10.1016/j.aquaeng.2014.11.003.

Wang, Q., Yu, Y., Zhang, Q., Zhang, X., Huang, H., Xiang, J., Li, F., 2019. Evaluation on the genomic selection in *Litopenaeus vannamei* for the resistance against *Vibrio parahaemolyticus*. Aquaculture 505, 212–216. https://doi.org/10.1016/j.aquaculture.2019.02.055.

Wang, X.A., Ma, A.J., Liu, Z.F., Sun, Z.B., Zhu, L.G., Chang, H.W., 2022. Genetic parameters estimation for growth traits in cultured tiger pufferfish (fugu), *Takifugu rubripes*. Acta Oceanol. Sin. 41 (12), 73–79. https://doi.org/10.1007/s13131-022-2058-5.

Yamamoto, T., Murashita, K., Matsunari, H., Oku, H., Furuita, H., Okamoto, H., Amano, S., Suzuki, N., 2016. Amago salmon *Oncorhynchus masou ishikawae* juveniles selectively bred for growth on a low fishmeal diet exhibit a good response to the low fishmeal diet due largely to an increased feed intake with a particular preference for the diet. Aquaculture 465, 380–386. https://doi.org/10.1016/j.aquaculture.2016.09.030.

Yáñez, J.M., Houston, R.D., Newman, S., 2014. Genetics and genomics of disease resistance in salmonid species. Front. Genet. 5, 415. https://doi.org/10.3389/fgene.2014.00415.

Yoshikawa, S., Chuda, H., Hamasaki, M., Kadomura, K., Yamada, T., Kikuchi, K., Hosoya, S., 2020. Precocious maturation in male tiger pufferfish *Takifugu rubripes*: genetics and endocrinology. Fish. Sci. 86 (2), 339–351. https://doi.org/10.1007/s12562-019-01390-4.

Yoshikawa, S., Hamasaki, M., Kadomura, K., Yamada, T., Chuda, H., Kikuchi, K., Hosoya, S., 2021. Genetic dissection of a precocious phenotype in male tiger pufferfish (*Takifugu rubripes*) using genotyping by random amplicon sequencing, direct (GRAS-Di). Mar. Biotechnol. 23 (2), 177–188. https://doi.org/10.1007/s10126-020-10013-4.

Yu, C., Fan, X., Hu, Z., Xia, X., Zhao, Y., Li, R., Bai, Y., 2020. Segmentation and measurement scheme for fish morphological features based on mask R-CNN. Inf. Process. Agric. 7, 523–534. https://doi.org/10.1016/j.inpa.2020.01.002.

Zenger, K.R., Khatkar, M.S., Jones, D.B., Khalilisamani, N., Jerry, D.R., Raadsma, H.W., 2019. Genomic selection in aquaculture: application, limitations and opportunities with special reference to marine shrimp and pearl oysters. Front. Genet. 9, 693. https://doi.org/10.3389/fgene.2018.00693.

Zhao, C., Chu, P., Liu, Y.X., Wang, S.J., Wang, T., Yin, S.W., 2024. Review on the reproductive biology of the genus and its application in sex control. Aquaculture 579, 740241. https://doi.org/10.1016/j.aquaculture.2023.740241.